

# Bridgman-grown $i\text{-Al}_{68.9}\text{Pd}_{21.6}\text{Mn}_{9.5}$ quasicrystal: Comparison of $\alpha$ , $C_p$ , $\sigma$ , and $\chi$ with those for flux-grown samples

C. A. Swenson,\* T. A. Lograsso, N. E. Anderson, Jr., and A. R. Ross†  
 Ames Laboratory, Iowa State University, Ames, Iowa 50011, USA

(Received 23 February 2004; published 17 September 2004)

Thermal expansivity ( $\alpha$ , 1–300 K), heat capacity ( $C_p$ , 1–108 K), electrical conductivity ( $\sigma$ , 1–300 K) and magnetic susceptibility ( $\chi$ , 1–300 K) data have been obtained for a Bridgman-grown single grain  $i\text{-Al}_{68.9}\text{Pd}_{21.6}\text{Mn}_{9.5}$  quasicrystal (BR) for direct comparison with data previously published for a flux-grown single grain sample [Phys. Rev. B **65**, 184206 (2002); PRB], and present  $\sigma$ ,  $\chi$  and  $C_p$  data for a second flux-grown sample described in an earlier publication [Philos. Mag. B **79**, 1673 (1999); PM]. Fortuitously, comparative analyses show these samples to have essentially the same composition. At all temperatures,  $\sigma$  and  $\chi$  for BR are, respectively, approximately one-third and one-quarter those for PRB. The  $C_p$ 's are the same ( $\pm 1\%$ ) down to 30 K, below which the BR  $C_p$  decreases more rapidly to one-half that for PRB at 1 K. The  $\alpha$ 's agree to  $\pm 2\%$  from 300 to 40 K, with a more rapid decrease for BR below 30 K, eventually to  $0.6 \alpha_{\text{PRB}}$  below 4 K. The total Grüneisen parameters are similar at all temperatures. The two methods for sample growth differ primarily in a quenching of the flux-grown sample to room temperature after growth, while the Bridgman-grown sample cools very slowly, resulting in slightly different phases, and magnetic properties which are associated with lattice defects. An attempt to convert the single grain flux-grown sample to the phase of the Bridgman sample using an  $800^\circ\text{C}$  anneal and a slow cool to room temperature was not successful, with the appearance of second phase inclusions. These inclusions are ascribed to slightly different compositions for the two phases [see Boissieu *et al.*, Philos. Mag. A **78**, 305 (1998)]. This suggests that a single grain flux-grown sample with an Mn composition near 9% cannot be converted by annealing and slow cooling into a single grain LT phase, and vice versa. These considerations may not apply to samples with Mn compositions closer to 8%.

DOI: 10.1103/PhysRevB.70.094201

PACS number(s): 61.44.Br, 62.20.Dc, 65.40.Ba, 65.40.De

## I. INTRODUCTION

Initially, quasicrystals, solids with long range symmetry but without normal crystalline periodicity, were metastable materials, and were discovered when certain binary alloys of Al and Mn, Cr, and Fe were cooled rapidly from a high temperature.<sup>1</sup> Subsequently, systems of ternary alloy quasicrystals were found which are stable at room temperature, and often can be obtained as large single grains.<sup>2</sup> Al-Pd-Mn alloys, which have been studied extensively, are one of these systems; see Ref. 3, where citations to previous work are given, together with linear thermal expansivity ( $\alpha$ ), heat capacity ( $C_p$ ), magnetic susceptibility ( $\chi$ ) and electrical resistivity ( $\rho$ ) data for flux-grown<sup>4</sup> single grain samples of quasicrystalline icosohedral AlPdMn (nominally  $i\text{-Al}_{71}\text{Pd}_{21}\text{Mn}_{08}$ ) and its  $\xi'$  (nonquasicrystalline) approximant. While the low temperature thermodynamic properties of most quasicrystals are well-behaved (though unusual; see Ref. 5), those for AlPdMn are complicated by the onset on cooling of a spin-glass associated with a small fraction (less than a few %) of the Mn.<sup>6–8</sup>

Préjean *et al.*<sup>8</sup> report low temperature  $\sigma(T) [= 1/\rho(T)]$  and  $\chi(T)$  data as a function of annealing rate for Czochralski-grown single grain  $i\text{-AlPdMn}$  samples [ICP (Inductively Coupled Plasma Atomic Emission Spectrometry) compositions  $\text{Al}_{70.5}\text{Pd}_{21.0}\text{Mn}_{8.5}$  and  $\text{Al}_{70.6}\text{Pd}_{21.5}\text{Mn}_{7.9}$ ]. They show that the electrical conductivity has a linear dependence on the (very small) number of magnetic Mn ions which determine  $\chi(T)$ ;  $\chi(T)$ , in turn, depends on the Mn composition of the sample and the cooling rate after annealing for three

hours at  $800^\circ\text{C}$ . In particular, the low temperature susceptibility (fraction of magnetic Mn ions) was 60% smaller when a sample initially at  $800^\circ\text{C}$  was cooled slowly ( $10^\circ\text{C}/\text{h}$ ) to room temperature than when it was quenched ( $150^\circ\text{C}/\text{min}$ ). This suggests that the low temperature thermodynamic properties of a flux-grown sample (as in Ref. 3), which is cooled rapidly to room temperature after growth,<sup>4</sup> should differ from those for a Bridgman<sup>9</sup>- or Czochralski-grown<sup>10,11</sup> sample, since these are cooled slowly to room temperature in the growth process; specifically, the Bridgman or Czochralski samples should show significantly smaller effects associated with the onset of the (magnetic) spin-glass state at low temperature. The present  $\alpha$ ,  $C_p$ ,  $\chi$  and  $\sigma$  data were taken for a large (10 mm, 1.6 g) single grain Bridgman-grown nominal  $i\text{-Al}_{69}\text{Pd}_{21}\text{Mn}_{10}$  sample for comparison with our earlier published results for a flux-grown single grain sample.<sup>3</sup>

The earliest report of the effects of composition and heat treatment on the physical properties of  $i\text{-AlPdMn}$  was by Lanco *et al.* who used  $\rho(T)$  and  $\chi(T)$  data from 4 to 300 K for melt-spun (quenched) samples of three different compositions to ascertain composition-dependent effects.<sup>12</sup> They showed that the magnitudes of  $\chi$  and of  $\rho$  and their temperature-dependences were very dependent on the Mn composition. For Mn contents of 7.5%, 8.5% and 10%, respectively,  $\chi$  at 200 K was  $-3$ ,  $0$ , and  $13 \times 10^{-7}$  emu/g, while the 4 K  $\rho$  ( $\rho_4$ ) decreased from 6400 to 3600 to 1600  $\mu\Omega\text{-cm}$ , with  $(\rho_4 - \rho_{300})$  decreasing from 3000 to 300 to (approximately) 0  $\mu\Omega\text{-cm}$ . Of relevance to the present results, they noted that  $\rho_4$  for the  $\text{Al}_{70.5}\text{Pd}_{22}\text{Mn}_{7.5}$  sample increased by 40% after warming slowly to and annealing at

970 K (700°C), then cooling at the same rate; corresponding  $\chi$  data were not reported. They ascribed this difference to an annealing effect.

Ishimasa and Mori<sup>13</sup> used electron microscopy to study the structure of AlPdMn samples (and also samples with an additional 1% to 3% Si) as a function of various heat treatments. They found that while samples grown from the melt (about 1180 K, 907°C), annealed at 1075 K (802°C), and quenched in water and liquid nitrogen, were standard F-type (F1, or HT) quasicrystals, samples which were given a second, lower temperature, anneal before being quenched showed a new low temperature equilibrium icosahedral phase (F2,  $F_{2M}$ , or, generically, LT) which involved a superlattice formation. The transition temperature is given as being between 1021 and 876 K (roughly between 750 and 600°C).

Audier *et al.*<sup>14</sup> used solidification sequences in ingots grown with both Bridgman and Czochralski techniques to determine the liquid AlPdMn phase diagram, and also noted the F1 to F2 (and  $F_{2M}$ ) transition region. In further investigations, Ishimasa,<sup>15</sup> Häußler *et al.*,<sup>16</sup> Boissieu *et al.*,<sup>17</sup> and Audier *et al.*<sup>18</sup> show that the equilibrium low temperature phase (LT) for compositions near  $\text{Al}_{70}\text{Pd}_{22}\text{Mn}_{08}$  cannot be described simply, and begins to form on cooling below 750°C (Ref. 18). Ishimasa<sup>15,19</sup> shows that quasicrystals with compositions close to  $\text{Al}_{71}\text{Pd}_{21}\text{Mn}_{08}$  which have been quenched to room temperature after a long period anneal at 600°C have a LT P-type phase rather than the F-type for other compositions. Boissieu *et al.*,<sup>17</sup> using samples from the experiments of Audier *et al.*,<sup>14</sup> give the relative compositions of the three phases as; HT icosahedral (F or F1) ( $\text{Al}_{68.8}\text{Pd}_{22.0}\text{Mn}_{9.2}$ ), lower temperature (intermediate) F2 ( $\text{Al}_{69.8}\text{Pd}_{21.4}\text{Mn}_{8.8}$ ) and (LT equilibrium)  $F_{2M}$  ( $\text{Al}_{69.3}\text{Pd}_{22.0}\text{Mn}_{8.7}$ ). The nominal (initial) composition of the Bridgman ingot from which these three samples were obtained was  $\text{Al}_{70.5}\text{Pd}_{22}\text{Mn}_{7.5}$ .<sup>18</sup>

The  $\chi$  investigations of Kobayashi *et al.*<sup>20</sup> ( $\text{Mn}_{10}$ , quenched) and Matsuo *et al.*<sup>21</sup> (nominal  $\text{Mn}_8$  and  $\text{Mn}_{8.5}$ ) involved temperature- and time-dependent effects from liquid helium temperatures to 600°C for samples which initially were quenched from 800°C to room temperature. The results are complex and are interpreted in terms of the discussion in the previous paragraph; a general result is that the low temperature  $\chi$  for the equilibrium LT state is appreciably smaller than that for the initial HT quenched-in state. Matsuo *et al.*<sup>21</sup> also show that after cycling to high temperature to obtain the equilibrium LT state, a subsequent anneal at 800°C and quench reproduces the initial, quenched  $\chi$ .

Rempel *et al.*<sup>22</sup> describe the magnetic properties of single grain Czochralski-grown  $\text{Al}_{70.2}\text{Pd}_{21.3}\text{Mn}_{8.5}$  from 4 to 1000 K and magnetic fields up to 50 kOe, including slight anisotropies. These suggest that their data, which qualitatively agree with post-annealing LT results given in Refs. 20 and 21, refer to the LT AlPdMn phase. The maximum temperature, 1000 K (727°C), fortuitously is below the 750°C temperature where the LT phase converts to the HT phase.<sup>18</sup> Their analysis of the low temperature magnetic data indicates that only 0.008% of the Mn ions are participating, which is appreciably smaller than that found earlier (1%–1.4%),<sup>6,7</sup> al-

though these  $\chi(T)$  data appear to be consistent with those of Préjean *et al.*,<sup>8</sup> who find this fraction for a comparable sample to be approximately 0.1%.

Hippert *et al.*<sup>23</sup> report the magnetic properties of a number of AlPdMn samples as a function of composition ( $\text{Mn}_{7.5}$  to  $\text{Mn}_{8.65}$ ), structure and thermal history. The temperature-dependences of these data have a common shape from approximately 6 K to 150 K when plotted as  $[\chi(T) - \chi(0)]/\mathbf{A}$ , where  $\chi(0)$  is a temperature-independent term, and  $\mathbf{A}^{24}$  is a scaling factor which is 1 for an arbitrary standard set of data and varies from 0.58 to 31.5 for the 19 samples. This correlation is, to a great extent, independent of sample structure and composition. The origin of the magnetism in AlPdMn in terms of essentially nondetectable sample inhomogeneities is discussed and an explanation of the deviations of  $\chi(T)$  from Curie-like behavior is given in terms of a Kondo effect competing with Ruderman-Kittel-Kasuya-Yosida (RKKY) interactions. Extensive citations are given to related experimental and theoretical literature.

## II. EXPERIMENTAL DETAILS

The data reported in the present paper involve *i*-AlPdMn samples from three different sources. Those for the flux-grown<sup>4</sup> single grain sample PRB (nominally  $\text{Al}_{71}\text{Pd}_{21}\text{Mn}_{08}$ ), unless otherwise noted, were published previously in Physical Review B.<sup>3</sup> Present data were taken for a Bridgman-grown single grain sample,<sup>25,26</sup> BR, and for a single grain flux-grown sample, PM, from material involved in an earlier Philosophical Magazine publication.<sup>4</sup>

Since the PRB and PM data were expected to characterize the quenched-in HT phase and the BR data the equilibrium LT phase, the logical next step was to transform the (HT) PRB sample to the LT state with a 72 h 800°C anneal and a slow cool (12°C/h) to room temperature (PRBAN). The resulting data were unusual (see below) and a subsequent metallographic analysis showed 2nd phase inclusions. Subsequent similar heat treatment (800°C anneal, slow cool) of a PRB resistivity sample ( $1 \times 1 \times 5 \text{ mm}^3$ ) showed the same effects, as did a BR resistivity sample after an 800°C anneal and quench to 300 K. When this BR sample was annealed again at 800°C and cooled slowly to 300 K, the inclusions disappeared. These effects can be interpreted using the difference between the compositions of the quenched-in HT 1 phase ( $\text{Al}_{68.8}\text{Pd}_{22.0}\text{Mn}_{9.2}$ ) and the LT ( $F_{2M}$ ) equilibrium phase ( $\text{Al}_{69.3}\text{Pd}_{22.0}\text{Mn}_{8.7}$ ) reported by Boissieu *et al.*<sup>17</sup> While generalizations probably are not appropriate, these results suggest that, for AlPdMn samples such as ours with approximately 9% Mn, the conversion of a single grain (quenched) HT sample to a single grain LT sample will involve a 0.5% increase in the Al composition and a 0.5% decrease in the Mn composition; that is, additional Al must be found, and 5% of the Mn must disappear. Clearly, this is not possible in a solid sample with a fixed (HT) composition. The inverse also must apply; a single grain LT sample cannot be converted to a single grain HT phase by annealing at 800°C and quenching. There are no indications of two-phase behavior in the systematic annealing studies of Préjean *et al.*,<sup>8</sup> who used Czochralski-grown single grain AlPdMn samples with 7.9%

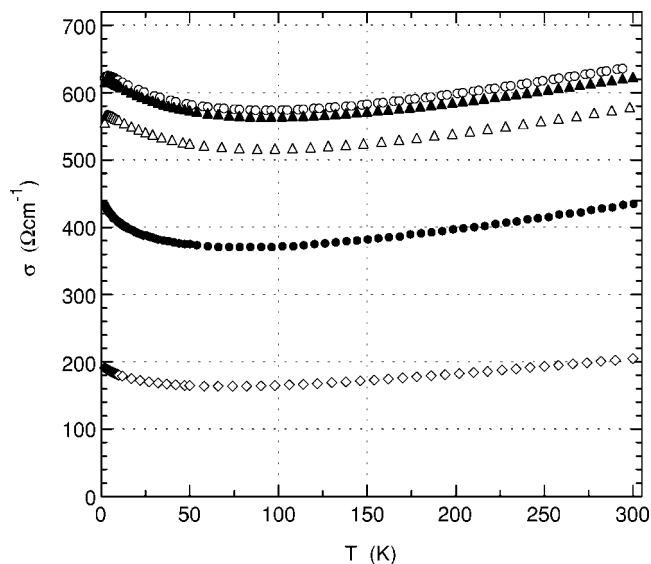


FIG. 1. Electrical conductivities ( $\sigma$ ) for the AlPdMn samples: ( $\blacktriangle$ ) PM, from Ref. 4. Present data: ( $\circ$ ) for PRB; ( $\triangle$ ) for PM; ( $\bullet$ ) for PRBAN; ( $\diamond$ ) for BR.

to 8.5% Mn. A possible explanation for the differences in these two experiments is given by the report of Ishimasa<sup>15,19</sup> that, for Mn compositions near 8%, the LT phase is P-type rather than the F-type for larger fractions.

Table I gives the compositions of these samples as determined by ICP (PRB, BR) and SEM (Scanning Electron Microscopy) (PRB, PM, BR) analyses. The SEM data (two series, I and II, different setups) were taken for samples mounted in close proximity on a common substrate to give reliable relative compositions. While no uncertainties are given for the ICP compositions, the SEM uncertainties reflect not only instrumental uncertainties but also deviations from an average of data taken at a number of points on the sample. The compositions of the three SEMI samples (fortuitously) are very similar, with the only significant difference occurring for the BR ICP composition which is barely within the

stated uncertainties; we have used a common molecular weight, 46.80 g/mol, in the analysis of the  $C_p$  data. The composition of the PRB sample as given in Table I is to be preferred to the estimate ( $\text{Al}_{71}\text{Pd}_{21}\text{Mn}_{08}$ ) in Ref. 3. Papers cited in Sec. I refer primarily to a nominal 8% Mn composition, so the larger Mn compositions in Table I may be significant in comparing results. See the end of the preceding paragraph and Secs. III A and III B

The BR(B) and BR(C) samples in Table I represent the two (equal, 30 mg) halves of a “resistivity” sample (1 mm<sup>2</sup> cross-section, 4 mm long) which was cut from the base of the Bridgman  $\alpha$  sample and was broken accidentally in preparations for a susceptibility ( $\chi$ ) measurement. The common compositions of the two halves of this sample are reassuring, but the differences from the BR SEMI composition are larger than expected; the PM sample was common to both SEM determinations. Subsequent metallographic inspection showed corresponding orientations for these two samples, and no evidence of a second phase. Table I also includes matrix and inclusion compositions for a portion of the PRBAN sample which was included inadvertently in the SEMII determinations.

The hardware and detailed procedures used for the  $\sigma$ ,  $\chi$ ,  $C_p$ , and  $\alpha$  measurements are identical with those described in earlier papers, and will not be repeated.<sup>3,5</sup> Susceptibility data were taken using a superconducting quantum interference device (SQUID) magnetometer. Since  $M(H)$  data to 70 kOe at 1.8 and 300 K showed linear behavior at low fields, the susceptibilities were determined from the measured moments  $M(T)$  using  $\chi(T) = M(T)/H$  with  $H = 1$  kOe. The precision of the conductivity data (sample dimensions approximately 1 mm  $\times$  1 mm  $\times$  5 mm) was better than 1%, with a systematic dimensional uncertainty of  $\pm 5\%$ . The  $C_p$  and  $\alpha$  samples were irregularly shaped, with a flat base and approximately 10 mm height to accommodate the dilatometer. The masses of the samples [PRB (PRBAN), PM, BR] were, respectively, 6.1, 4, and 1.6 g. The  $C_p$  data were taken from 1 to 108 K using a standard tray-type isothermal calorimeter,<sup>27</sup> while the 1 to 300 K  $\alpha$  data were obtained using a differential capaci-

TABLE I. Sample Compositions (in Atomic %) from ICP and (relative) SEM analyses; the corresponding molecular weights are given in grams. The SEMI and the SEMII data were taken on common (but different) substrates; the same PM sample was used in the two determinations. BR(B) and BR(C) are the two halves of the broken resistivity sample. See the text for details.

Sample	Al	Pd	Mn	Mol Wt
PRB ICP	68.93	21.62	9.45	46.80
PRB SEMI	68.9(5)	21.6(2)	9.5(2)	46.8(5)
PM SEMI	69.0(3)	21.0(1)	9.9(2)	46.5(2)
PM SEMII	69.8(3)	20.9(3)	9.4(2)	46.2(4)
BR ICP	69.22	20.73	10.05	46.26
BR SEMI	69.1(3)	21.5 (4)	9.4(5)	46.7(5)
BR(B) SEMII	70.1(3)	20.1(2)	9.8(1)	45.7(4)
BR(C) SEMII	70.3(2)	19.9(4)	9.8(3)	45.5(4)
PRBAN(2-phase) SEMII				
Matrix	68.6(3)	22.1(4)	9.4(3)	47.2
Inclusions	73.5(3)	19.6(4)	7.0(4)	44.5

tance dilatometer which was calibrated using a high purity copper standard.<sup>28</sup>

### III. EXPERIMENTAL RESULTS

#### A. Electrical conductivities

Figure 1 gives the temperature-dependences of the electrical conductivities of the present samples. The conductivities of the three single grain self-flux-grown samples [(▲) from Ref. 4, and present data for this same PM material (△) and for PRB (○)] essentially are in agreement within the 5% systematic uncertainty in these data. The conductivities of the BR sample (◇) are significantly smaller than those for the flux-grown samples, in agreement with the results of Préjean *et al.*<sup>8</sup> When compared with those data, the slightly smaller conductivities and temperature-dependences of the present data probably are associated with the larger Mn content [Mn<sub>9.5(3)</sub> vs Mn<sub>8.2(3)</sub>].<sup>12</sup> The two-phase PRBAN (•) data lie between these two.

#### B. Magnetic Susceptibilities

Figures 2 present the magnetic susceptibility ( $\chi$ ) data for the samples which are characterized in Table I. At “high” temperatures,  $\chi$  is expected to show a Curie-Weiss type behavior

$$\chi = \chi_0 + C/(T - \theta). \quad (1)$$

where  $C$  is the Curie constant,  $\theta$  the Curie-Weiss temperature, and  $\chi_0$  a temperature-independent term, often diamagnetic ( $<0$ ). Table II gives parameters for fits of Eq. (1) to both the high  $T$  ( $100 \leq T \leq 300$  K) and low  $T$  ( $T < 30$  K) data; STD represents the standard deviations of the data from the fits. The minima which determine these fits for the high  $T$  data are very shallow; the numbers in parentheses for these parameters show the effect of  $\delta\theta = +1$  K on the other parameters. The magnitudes of  $\chi$  for the flux-grown samples (PRB, PRBAN, PM) are significantly larger than those for the Bridgman-grown samples (BR), leading to the different  $y$ -axis scales in Fig. 2. The values of  $\chi$  at 300 K (not shown) vary from 7 to  $2 \times 10^{-7}$  emu/g for the flux-grown samples to  $-1.5 \times 10^{-7}$  emu/g for the average of the fits to the BR(B) and BR(C) data [BR(BC)];  $\chi = 0$  at 150 K for BR(BC). The very strong Mn dependence of  $\chi$  noted by Lanco *et al.*<sup>12</sup> and Lasjaunias *et al.*<sup>7</sup> is qualitatively consistent with the relative differences (an order of magnitude) between the low  $T$   $\chi$ 's for the 7.9% and 8.5% Mn samples of Préjean *et al.*<sup>8</sup> (their Fig. 1), which were selected to have small magnetic effects, and the low  $T$  data for the current (9.5% Mn) samples [Fig. 2(b)]. The high  $T$  fits of Eq. (1) to the data could have been extended down to 65 K with a slight loss of precision, but the practical upper limit of the low  $T$  fits was approximately 35 K. Hippert *et al.*<sup>23</sup> (and, earlier, Ref. 8) ascribe the inability to represent AlPdMn susceptibility data with Eq. (1) to the existence of a Kondo effect competing with RKKY interactions, which, when included, allows the representation their data from 5 to 150 K. Hence, the parameters in Table II have no direct physical significance, and are useful primarily

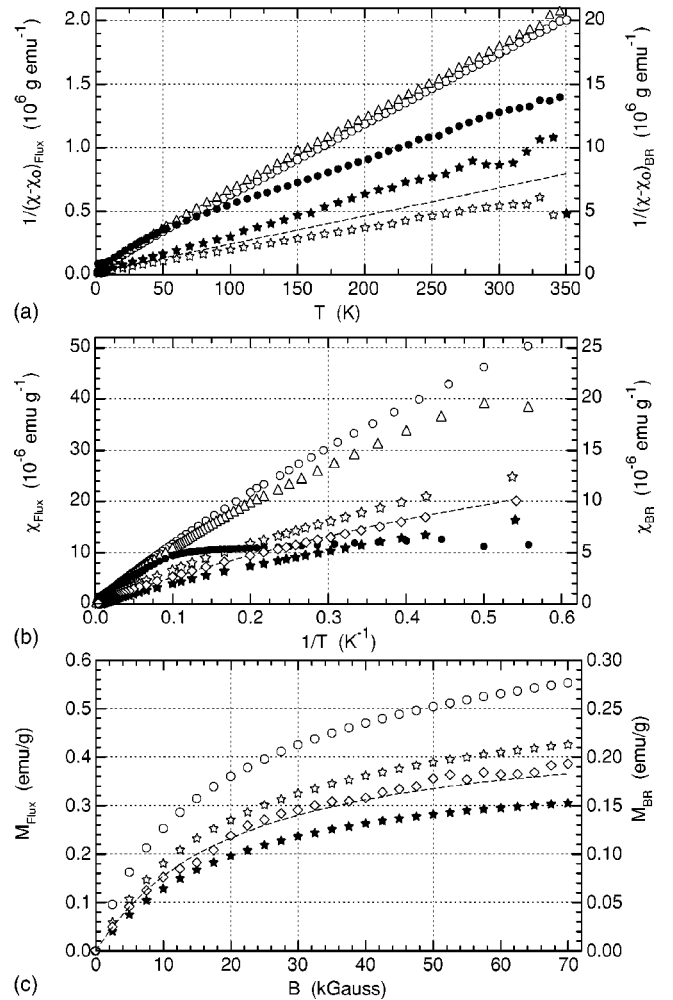


FIG. 2. Magnetic data for the AlPdMn samples: Fig. 2(a),  $1/[\chi(T) - \chi_0]$  vs  $T$ ; Fig. 2(b),  $\chi(T)$  vs  $1/T$ ; Fig. 2(c), magnetic moment  $M$  as a function of field  $H$  at 1.85 K. Symbols are as for Fig. 1, with: Open and solid (☆) representing individual data for BR(B) and BR(C), respectively; (---) in Figs. 2 are a smooth average of the BR(B) and BR(C) data; in Figs. 2(b) and 2(c), (◇) are actual data for the combined BR(B) and BR(C) samples. In these figures, the flux-grown [PRB (○), PRBAN (•), PM (△)] data use the left-hand and the smaller Bridgman (BR) [(◇), open and solid (☆)] data the right-hand scales. See the text for details.

to represent the data (from 100 to 300 K, and 2 to 30 K, respectively). In particular, for a dilute magnetic system such as exists for AlPdMn,  $\theta$  should be zero.

Figure 2(a) provides a test of Eq. (1), with  $1/[\chi(T) - \chi_0]$  approximately linear in  $T$  for temperatures above 65 K, and the slopes inversely related to the  $C$ 's in Table II. At low temperatures,  $\chi_0$  is negligible, and the data are best presented by  $\chi(1/T)$  in Fig. 2(b). This figure contains the data (◇) which were obtained when the BR(B) and BR(C) samples were combined into a single sample, as well as the average (---) [BR(BC)] of the fits of Eq. (1) to these data. The agreement is quite satisfactory, and gives the basis for using BR(BC) to represent the susceptibility at higher temperatures. For unknown reasons, the  $\chi(T)$  data for high  $T$  were much better for the individual BR pieces than for the combination (not

TABLE II. Parameters for fits of Eq. (1) to the susceptibility data for the various samples in Fig. 2. See the text for details.

Sample	$\theta$ K	C $10^{-4}$ emu-K/g	$\chi_0$ $10^{-7}$ emu/g	STD $10^{-9}$ emu/g
$T > 100$ K				
PRB	-20.4(10)	1.772(18)	-0.06(-4)	0.704(1)
PM	-12.5(10)	1.795(20)	-2.96(-5)	0.97(12)
PRBAN	-55.0(10)	2.82(2)	-0.37(-5)	9.19(5)
BR(B)	-18.3(10)	0.610(6)	-2.55(-2)	4.67(1)
BR(C)	0.5(10)	0.313(4)	-3.07(-1)	7.29(1)
BR(BC)	-9.9(10)	0.455(5)	-2.80(-1)	0.02(13)
$T < 30$ K				
PRB	-1.2	1.23	1.20	373
PM	-0.60	1.19	4.10	92
BR(B)	-0.88	0.334	1.54	54
BR(C)	-0.79	0.214	-0.27	32
BR(BC)	-0.85	0.274	0.64	0.05

shown). Figure 2(c) gives the corresponding 1.85 K field dependence of the magnetic moment for these BR samples, as well as for the PRB sample. Again, the average of the data for BR(B) and BR(C) (---) agrees well with the actual data for the combined sample ( $\diamond$ ). In each of Figs. 2(a) and 2(b),  $\chi(T)$  for the two-phase sample [PRBAN, ( $\bullet$ )] has a quite different shape from that for the single phase samples. Note that the average of the ratio of the values of C for the high and low T fits for PRB, PM and BR(BC) in Table II is 1.53,<sup>10</sup> and is consistent with that from Rempel *et al.*,<sup>22</sup> 1.65.

The differences between the  $\chi$ 's of BR(B) and BR(C) present a puzzle. They are the two halves of the sample which was used to obtain the BR conductivity data shown in Fig. 1, have identical compositions (Table I), and metallographic inspection shows them to be single phase with a common orientation across the break (no grain boundary). The differences are not experimental, since  $\chi(1/T)$  [Fig. 2(b)] and low temperature  $M(H)$  [Fig. 2(c)] data for a combination of the two samples are consistent with the sum of the individual data. Following Préjean *et al.*,<sup>8</sup> but using the high  $T$  values of  $C$  in Table II, the fraction of the Mn ions which are magnetic can be estimated to be 0.35% and 0.67% for these two samples. The possibility of a localization or highly nonuniform distribution of the magnetic ions is suggested by these data.

### C. Representation of $C_p$ and $\alpha$ data

The bases for the presentation of the present  $C_p$  and  $\alpha$  data are given in previous papers,<sup>3,5</sup> and are summarized in the following. The basic equations used to represent low temperature data are:

$$C_p/T = \sum_{n=0}^N C_{2n+1} T^{2n}, \quad (2a)$$

$$\alpha/T = \sum_{n=0}^N A_{2n+1} T^{2n}. \quad (2b)$$

The lead parameters,  $C_1$  and  $A_1$ , generally are ascribed to electronic contributions, with  $C_1 = \gamma$ , the electronic specific heat coefficient, although, for amorphous solids, a linear term also has been associated with a distribution of tunneling states.<sup>29</sup> In most instances, higher order terms are associated with lattice properties ( $C_p^{\text{lat}}$ ), with the characteristic  $T=0$  Debye temperature  $\Theta_0$  given by<sup>30</sup>

$$\begin{aligned} \Theta_0^3 &= [(12\pi^4/5)rR/C_3] \\ &= [1.944 \times 10^6 r(\text{mJ/g} - \text{mol} - \text{K})/C_3] \text{K}^3, \end{aligned} \quad (3)$$

where  $R$  and  $r$  are the gas constant and the number of atoms per unit cell, respectively. This equation has no significance for tunneling systems, where the "lattice" contribution,  $C_3$ , often is appreciably greater than would be calculated for a Debye solid.<sup>29</sup>

$\Theta_0$  also can be calculated from an average 0 K sound velocity as<sup>30</sup>

$$(\Theta_0^{\text{el}})^3 = (h/k_B)^3 (3rN_0/4\pi V_m) (1/(1/v^3)), \quad (4a)$$

which for a quasicrystal (isotropic, only two sound velocities;  $v_L$  and a twofold degenerate  $v_T$ ) is

$$= (h/k_B)^3 (3rN_0/4\pi V_m) v_T^3 [3/(2 + (v_T/v_L)^3)] \quad (4b)$$

$$= (2.5142 \times 10^{-3})^3 (r/V_m) v_T^3 [3/(2 + (v_T/v_L)^3)], \quad (4c)$$

where  $h$  is Planck's constant,  $k_B$  the Boltzman constant,  $N_0$  Avagadro's number (/g-mol),  $V_m$  the molar volume [ $\text{m}^3/(\text{g-mol})$ ],  $r$  as above, and the sound velocities are in m/s. These velocities are related to the elastic constants as  $C_T = C_{44} = \rho v_T^2$ , and  $C_L = C_{11} = \rho v_L^2$ . Note that the density,  $\rho$ , enters into Eqs. (4) only through the definition of the molar volume.

The onset of the spin-glass state below approximately 10 K (Ref. 3) masks the behavior implied by Eqs. (2), and makes it impossible to determine  $\Theta_0$  and  $\gamma$  through fits to  $C_p(T)$  data for *i*-AlPdMn. For convenience, power series similar to Eqs.(2) were used to represent the data, with  $T^n$  rather than  $T^{2n}$ ; the parameters for these series have no physical significance.

At low temperatures (below  $\Theta_0/10$ ), the rapid temperature-dependence of  $C_p$  presents difficulties in the display of data. Since the Debye function approximates this temperature dependence, it is reasonable to use the Debye function as the basis for displaying  $C_p$  results; one procedure for accomplishing this is to relate experimental lattice  $C_V(T)$ 's [ $C_V^{\text{lat}} = C_V(T) - \gamma T$ ]<sup>31</sup> directly to the Debye function using equivalent Debye  $\Theta$ 's.<sup>32</sup> For a  $C_V^{\text{lat}}$  datum at  $T$ ,  $\Theta(T)$  is the Debye temperature which, when used in the Debye relation for  $C_V$  ( $C_{\text{Debye}}$ , Ref. 30), will give the same  $C_V^{\text{lat}}$  at that temperature

$$C_V^{\text{lat}}(T) = C_V(T) - \gamma T = C_{\text{Debye}}[\Theta(T)/T]. \quad (5)$$

A plot of  $\Theta(T)$  vs  $T$  shows deviations of the data from the Debye function, or the effects of dispersion (non-Debye-like behavior); a decreasing  $\Theta$  represents an increasing positive deviation of  $C_V$  from Debye behavior. When comparing materials with significantly different  $\Theta_0$ 's, a normalized plot of  $\Theta(T)/\Theta_0$  vs  $T/\Theta_0$  will display clearly differences in the shapes of the  $C_V(T)$  relations and forms the basis for the normalization of the  $T > 20$  K PRB  $C_p$  data to non-magnetic AlPdMn  $\xi'$  approximant  $C_p$  data to obtain an estimate of the *i*-AlPdMn lattice  $C_p(T)$  at lower temperatures.<sup>3</sup>

The volume thermal expansivity ( $\beta = 3\alpha$  for an isotropic solid) is related directly to  $C_V(T)$  by the Grüneisen relation,<sup>32,33</sup>

$$\beta = 3\alpha = \Gamma(C_V/B_T V) = \Gamma(C_p/B_S V), \quad (6a)$$

where  $B_T$  and  $B_S$  are the isothermal and adiabatic bulk moduli,  $V$  is the molar volume,  $\Gamma$  is the dimensionless Grüneisen parameter, and  $C_p/C_V = B_S/B_T$ .<sup>31</sup> If independent (separable) contributions to the thermodynamics of an isotropic solid can be identified (such as electronic, lattice, magnetic, spin-glass, etc.), each contribution will have a  $C_{Vi}$  and a  $\Gamma_i$  associated with it, and the individual thermal expansivities will be additive to give for an isotropic material

$$\beta = \sum \beta_i = 3 \sum \alpha_i = \sum \Gamma_i C_{Vi} / B_T V. \quad (6b)$$

In this model, the  $\Gamma_i$ 's are given by

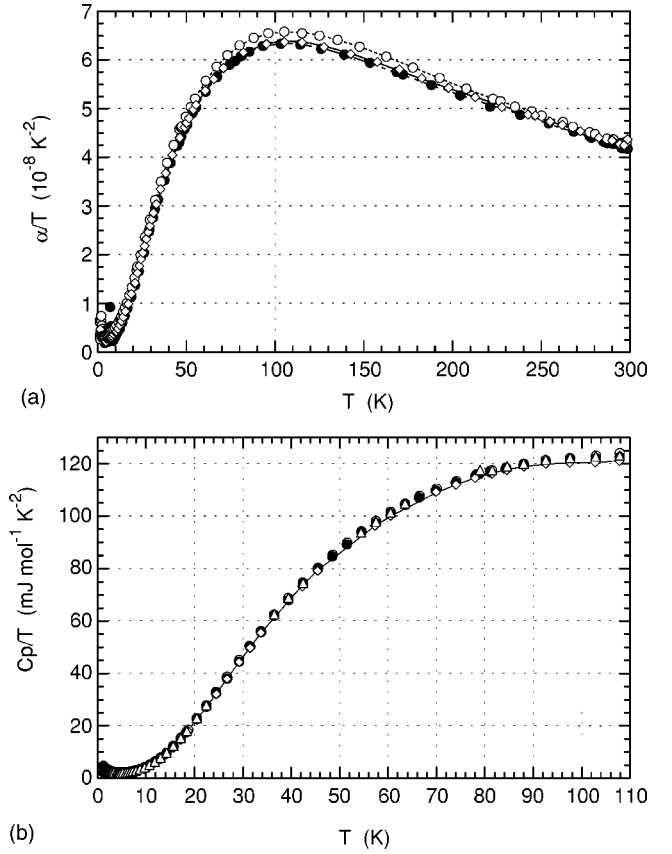


FIG. 3.  $\alpha/T$  (a) and  $C_p/T$  (b) vs  $T$  data for Al-Pd-Mn quasicrystals: ( $\circ$ ) PRB, data from Ref. 3; ( $\bullet$ ), present annealed PRB (PRBAN); ( $\diamond$ ) present BR; ( $\triangle$ ) present PM  $C_p(T)$  (sample from Ref. 4). The lines, where shown, represent fits to the data. The  $C_p$  data are indistinguishable in Fig. 3(b). The  $T$  scales are different for the two figures.

$$\Gamma_i = 3B_T V (\alpha_i / C_{Vi}) = -d \ln \Phi_i / d \ln V, \quad (7)$$

where the characteristic energy,  $\Phi_i$ , may be  $\Theta_0$  for the lattice, the Fermi Energy for free electrons, the Curie temperature for a magnetic system, etc. Values of  $\Gamma$  typically range from  $\pm 1$  to  $\pm 4$  (Ref. 33), although  $\Gamma$  will have much larger magnitudes when  $\Phi$  has a large volume sensitivity, such as that associated with tunnelling.<sup>29,33</sup> The lattice  $\Gamma$ ,  $\Gamma^{\text{lat}}$ , generally has a temperature-dependence similar to that of  $\Theta(T)$ , since the lattice modes which are excited with increasing  $T$  may have significantly different volume-dependences. By analogy with  $\Theta(T)$ ,  $\Gamma_0^{\text{lat}}$  is the limiting,  $T=0$  value of  $\Gamma^{\text{lat}}(T)$ , and, at high  $T$ ,  $\Gamma^{\text{lat}}$  approaches a constant value,  $\Gamma_\infty^{\text{lat}}$ . Since  $\Gamma_0^{\text{lat}} = -d \ln \Theta_0 / d \ln V$ ,  $\Gamma_0^{\text{lat}}$  also can be calculated from the volume-(pressure-) dependence of the sound velocities [Eqs. (4).

#### D. $C_p$ and $\alpha$ data

Figures 3, in which the  $\alpha$  and  $C_p$  data have been normalized by  $T$  to compensate partially for their rapid temperature-dependence, present an overall picture of these data, while Figs. 4 use the format suggested by Eqs. (2) to display the low temperature data. The  $\Theta(T)$  plot in Fig. 5, which is

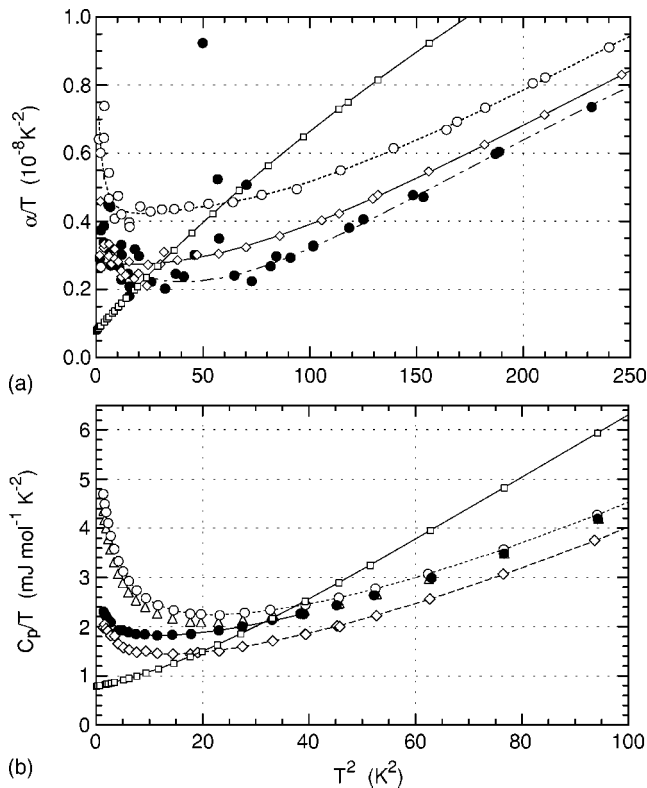


FIG. 4.  $\alpha/T$  (a) and  $C_p/T$  (b) vs  $T^2$  for the lower temperature data in Fig. 3. Symbols are as for Fig. 3, with  $(-\square-)$  smooth representations of the AlPdMn  $\xi'$  approximant data from Ref. 3. The  $T^2$  scales are different for the two figures.

based on the Debye  $C_p$  function [Eq. (5)], provides a more sensitive presentation of the data from 7 to 105 K; between 15 and 40 K, the marker sizes correspond to approximately 5% in  $C_p$ . In these figures, data for the flux-grown PRB ( $\circ$ ) sample are from Ref. 3, with present data shown for the Bridgman-grown sample [BR, ( $\diamond$ )], the two-phase PRBAN sample ( $\bullet$ ), and  $C_p$  only for the flux-grown PM material described in Ref. 4 ( $\triangle$ ).

Smooth AlPdMn  $\xi'$  approximant data from Ref. 3 are shown in Figs. 4 ( $-\square-$ ) to illustrate for a similar material the temperature-dependences of  $\alpha/T$  and  $C_p/T$  in the absence of the spin-glass contribution; spin-glass contributions to the quasicrystal  $\alpha$  and  $C_p$  data clearly are important. In Ref. 3, the shapes of the quasicrystal PRB and  $\xi'$  approximant  $C_p(T)$  relations are very similar above 20 K, which allowed the approximant data to be normalized to the quasicrystal data from 20 to 105 K and extrapolated to lower temperatures to approximate the behavior of a similar nonspin glass quasicrystal [see the discussion following Eq. (5)]. This normalized  $\Theta(T)$  for the approximant is shown in Fig. 5 ( $-\square-$ ) to illustrate qualitatively the effect of the spin-glass state on  $C_p$  for the quasicrystals. The value of  $\Theta_0$  for PRB as calculated from the elastic constants [Eqs. (4)],  $\Theta_0^{el} = 505(1)$  K (Ref. 3), also is shown in Fig. 5 to provide qualitative confirmation that the shape of the normalized relation is relevant; the larger  $\Theta_0$  and systematically larger  $\Theta$ 's from 10 to 20 K for all of the quasicrystals suggest that PRB is elastically more rigid than the approximant,<sup>3</sup> since, for a fixed  $T$ , a larger  $\Theta$  corresponds to a smaller  $C_p$ .

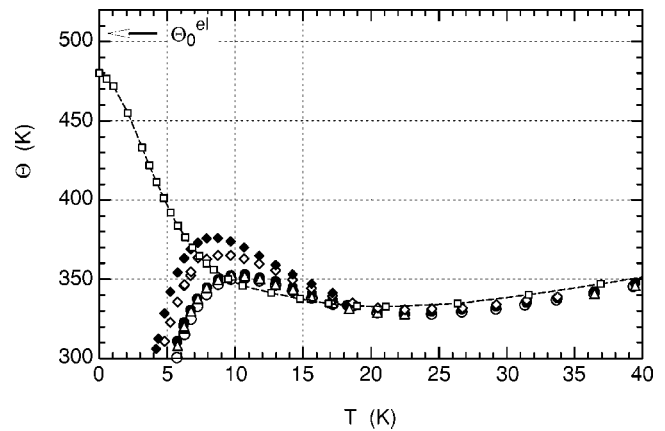


FIG. 5. An equivalent Debye theta [ $\Theta(T)$ , Eq. (5)] representation of the  $C_p(T)$  data, with symbols as in Fig. 3(b); here,  $(-\square-)$  is from a normalization of the high  $T$  AlPdMn  $\xi'$  approximant  $C_p$  data to the PRB data, from Ref. 3. ( $\blacklozenge$ ) are a recalculation of the BR data assuming  $\gamma = 0.25$   $\text{mJ mol}^{-1} \text{K}^{-2}$ .  $\Theta_0^{el} = 505$  K is from Ref. 3. See the text for details.

All of the quasicrystal  $C_p$  data are in essential agreement ( $\pm 1\%$ ) above 30 K [Figs. 3(b) and 5], with differences appearing at lower temperatures [Figs. 4(b) and 5] which, for PRB, PM and BR can be associated with differences in the spin-glass contribution, and, for PRBAN, this contribution plus the second phase. When compared to PRB ( $\circ$ ),  $C_p(T)$ 's for the (very similar) PM sample ( $\triangle$ ) and for the two-phase PRBAN ( $\bullet$ ) show deviations below 9 K, with 1 K magnitudes 94% and 48%, respectively, of PRB [see Fig. 4(b)]. The BR  $C_p$  data ( $\diamond$ ) begin to deviate from those for PRB below 30 K, with the differences becoming significant ( $\sim 5\%$ ) below 20, and are 47% of  $C_p$  for PRB at 1 K.

A comparison with the normalized approximant data suggests that the lattice contribution to  $C_p$  is only a few percent at 3 K and rapidly becomes negligible at lower temperatures,<sup>3</sup> so the relative 1 K magnitudes of  $C_p/T$  for PRB, PM and BR can be associated with differences in the magnetic (spin-glass) contribution and should be related to the corresponding values of  $\chi$  in Fig. 2(b) (Table II). The relationship is not direct, since in Table II, the ratio of the Curie parameters ( $C$ ) is approximately 4, while the corresponding 1 K  $C_p$  ratio is close to 2. The small differences between the PM ( $\triangle$ ) and PRB ( $\circ$ )  $C_p$ 's which occur below 9 K (to  $-6\%$  below 4 K) possibly are related qualitatively to the relative low temperature values of  $C$  in Table II [see Fig. 2(b)]. No obvious explanation exists for the temperature-dependence of  $C_p$  for two-phase PRBAN, which, on cooling, deviates from that for PRB at approximately the same temperature as the break in the  $\chi(1/T)$  relation in Fig. 2(b); this break suggests magnetic ordering below 10 K. The composition of the matrix in PRBAN is approximately that of the other quasicrystals (Table I).

In Ref. 3, the maximum in  $\Theta$  (or, more correctly, the inflection point) for PRB (see Fig. 5, approximately 11 K) was associated with the onset of the spin-glass contribution, but the differences between PRB and BR (previous paragraph) suggest a higher temperature (20 to 30 K). For all of these data, a possible electronic contribution to the quasi-

crystal  $C_p$  has been ignored [ $\gamma=0$  in Eq. (5)]. The ( $\blacklozenge$ ) symbols in Fig. 5 show the effect on  $\Theta(T)$  for BR when a “reasonable” value for  $\gamma$  ( $=0.25$  mJ/mol-K<sup>2</sup>, Ref. 3) is assumed. The difference is significant, but affects only slightly the estimated temperature for the onset of spin-glass effects.

A discussion of previous  $C_p$  and  $\alpha$  data is given in Ref. 3. The low temperature  $C_p$  data for PRB agree well with those of Chernikov *et al.* for a quenched nominal  $i$ -Al<sub>70</sub>Pd<sub>21</sub>Mn<sub>09</sub> sample.<sup>34</sup> Although their 1.9 K M(H) data are very similar to those in Fig. 2(c), the data from 50 to 200 K were represented by a Curie constant ( $C=7 \times 10^{-4}$  emu/g) and Curie-Weiss parameter ( $\theta=-108$  K) which are very different from those for PRB in Table II. The differences from the present  $C_p$  data of the 1 to 7 K data for a Bridgman-grown sample (nominally  $i$ -Al<sub>69.5</sub>Pd<sub>21.5</sub>Mn<sub>9.5</sub>) from Lasjaunias *et al.*<sup>7</sup> are larger, possibly because of the higher Mn content.<sup>35</sup> This would be consistent with a low temperature  $C=1.6 \times 10^{-4}$  emu/g which is appreciably larger than those for the flux samples in Table II, and with M(H) at 2 K also larger than those in Fig. 2(c).<sup>7</sup>

The  $\alpha$ 's for PRB ( $\circ$ ) in Figs. 3(a) and 4(a) are from Ref. 3, while those for BR ( $\diamond$ ) and PRBAN ( $\bullet$ ) are present data;  $\alpha$  data were not taken for the PM  $C_p$  sample. As for the  $C_p$  data, the  $\alpha$  data are in reasonable agreement ( $\pm 2\%$ ) from 300 to 45 K; at lower temperatures, the BR (and PRBAN) data show a significantly stronger temperature-dependence than those for PRB and, below 5 K, are only 60% of  $\alpha_{\text{PRB}}$  [Fig. 4(a)]. The BR and PRB  $\alpha(T)$  data show approximately the expected dilatometer precision ( $\pm 10^{-9}$  K<sup>-1</sup>, Ref. 3). As for the  $C_p$  data in Fig. 4(b), the shapes of the  $\alpha(T)/T$  relations are similar for BR and PRB, but, because of spin-glass formation, are qualitatively different from those of the  $\xi'$  approximant ( $-\square-$ ). Reference 3 discusses previous AlPdMn thermal expansivity data, none of which have comparable accuracy at low temperature.

The  $\alpha$  data for the two-phase annealed PRB (PRBAN) sample Figure 4(a) are not of the same quality as those for PRB and BR, and, although in agreement ( $-1\%$ ) with those for BR above 40 K, show excess scatter below 10 K, as well as a reproducible spike near 7 K ( $T^2=50$  K<sup>2</sup>). At higher temperatures, small isothermal drifts (sample shortening) appeared on warming and data-taking was not possible from 35 to 50 K. An anneal at 50 K and an overnight cooling to 28 K allowed drift free data to be taken to 56 K, which were in agreement with earlier data taken on cooling from 300 K. In contrast, the  $C_p$  data for this sample (which initially was cooled slowly from 77 to 4 K) show smooth behavior ( $\pm 1\%$ ) at all temperatures, and only deviated from  $C_p$  for PRB below 10 K [Fig. 4(b)].

The Grüneisen parameter [ $\Gamma$ , Eqs. (6a) and (6b)] provides a dimensionless relationship between  $C_p$  and  $\alpha$  and a measure of the volume-dependences of the characteristic energies of a material [Eq. (7)]. Figure 6 gives the temperature dependence of the total  $\Gamma$  (ignoring specific electronic contributions) for PRB ( $\circ$ ), BR ( $\diamond$ ) and PRBAN ( $\bullet$ ); here, actual  $\alpha$  data and smooth representations of  $C_p(T)$  were used to calculate  $\Gamma(T)$  for each sample, with  $3B_T V=3.41 \times 10^9$  mJ/g-mol (Ref. 3, corrected for the molar volume in Table I). The scatter in  $\Gamma(T)$  reflects sensitively the relative

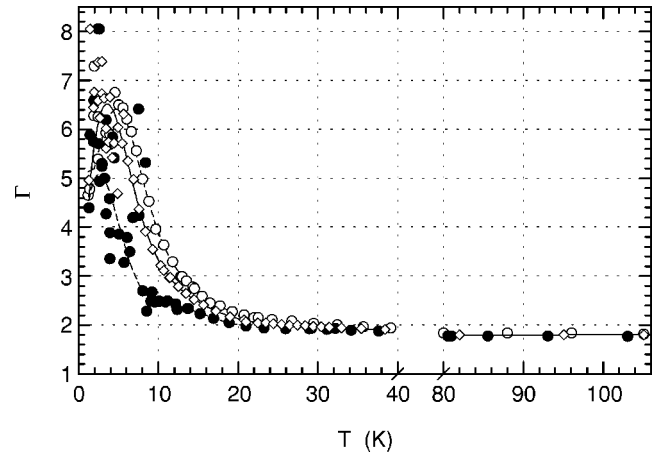


FIG. 6. Total Grüneisen parameters,  $\Gamma$ , for the thermal expansion samples, with symbols as in Figs. 3. Note the split temperature scale.

scatter in the  $\alpha$  data; contrast the behavior of the PRBAN data ( $\bullet$ ) and that of the other two samples.  $\Gamma_{\text{PRB}}$  and  $\Gamma_{\text{BR}}$  are in essential agreement above 15 K, where spin-glass contributions are small, and below 6 K, where spin-glass contributions predominate for both samples, with  $\Gamma$  at 1 K giving  $\Gamma_{\text{spin-glass}}=6(1)$ . In Fig. 6, the small differences in  $\Gamma$  at intermediate temperatures is a result of the relatively smaller BR spin-glass contribution. The implication is that  $\Gamma(T)$  in the absence of spin-glass effects increases rapidly as the temperature decreases.

$\Gamma(T)$  in Fig. 6 is constant at above 50 K, but begins to increase with decreasing temperature at lower temperatures. This behavior is unusual, since an increase in  $\Gamma$  with decreasing temperature usually occurs at temperatures approaching the minimum in  $\Theta(T)$  (25 K in Fig. 5). The basis for this rapid increase in  $\Gamma$  with decreasing temperature is shown in Fig. 7, where  $\alpha(T)/T$  and  $C_p(T)/T$  have closely similar shapes, but at all temperatures (to 25 K),  $\alpha(T)$  is offset by a relatively large contribution linear in  $T$  (see Eqs. (2)).

#### IV. DISCUSSION/SUMMARY

The initial objective of the present experiments was to obtain  $C_p(T)$  and  $\alpha(T)$  data for a single grain Bridgman-grown AlPdMn quasicrystal (BR) for comparison with previous data for a similar single grain flux-grown AlPdMn quasicrystal (PRB).<sup>3</sup> The primary difference between these materials is that the final flux-grown sample is quenched from the growth temperature (800+ °C) to room temperature, while the Bridgman-grown sample is cooled very slowly from the same temperatures and should have smaller inhomogeneities. Low temperature  $C_p$  and  $\alpha$  data for AlPdMn quasicrystals show an anomalous contribution (that is, a deviation from normal lattice or metallic behavior) which is ascribed to the onset of a spin-glass which is associated with the magnetism of a small fraction of the Mn ions;<sup>3,6,7</sup> these magnetic ions, in turn, are related to inhomogeneities (defects) in the material.<sup>8,23</sup> The low temperature  $\chi(T)$  gives a direct measure of this magnetism, and the re-

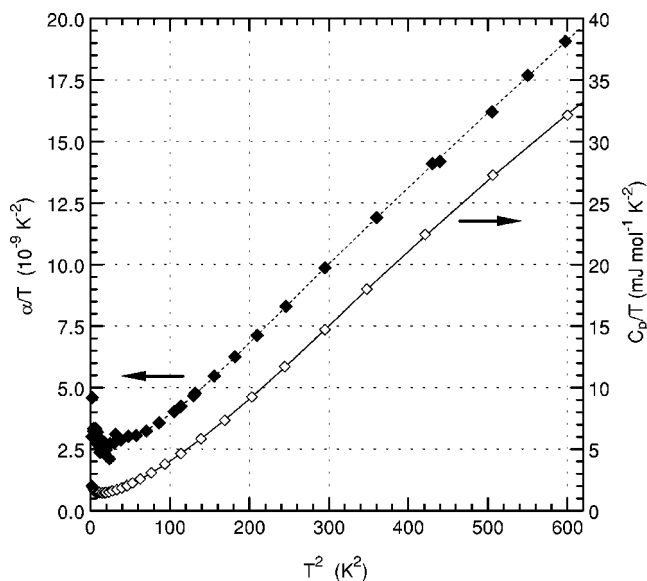


FIG. 7. A comparison of  $\alpha/T$  and  $C_p/T$  vs  $T^2$  for the single-grain Bridgman sample. The ( $\blacklozenge$ ) represent  $\alpha/T$  (left scale), the ( $\diamond$ )  $C_p/T$  (right scale).

sults of Prejean *et al.*<sup>8</sup> and Hippert *et al.*<sup>23</sup> show that  $\chi$  is sensitive to both annealing procedures and, presumably, Mn composition. Fortunately, our three samples (see Table I) have very similar compositions, so differences between the flux-grown (PRB, PM) and Bridgman-grown (BR) samples would be expected to be associated primarily with a smaller concentrations of defects for the latter.

Figures 3 and 4 present the  $C_p$  and  $\alpha$  data for the flux-grown ( $\circ, \Delta$ ) and Bridgman-grown ( $\Delta$ ) samples. While the  $C_p$  and  $\alpha$  are very similar for all samples above 25 K, the BR data in each case are smaller than those for the flux-grown samples at lower temperatures, in qualitative agreement with the decreased susceptibilities in Table II and Fig. 2. Thus, the effects of spin-glass formation become significant on cooling below 25(5) K for the flux-grown PRB, and, from Fig. 5, near 15 K for BR.

In Fig. 5, the  $\Theta(T)$  relations for the experimental data were calculated from the total  $C_p$  data, neglecting electronic contributions [ $\gamma=0$  in Eq. (5)]. The relatively small effect of including these is shown by a recalculation of the BR relation using a “reasonable” value of  $\gamma$  ( $\blacklozenge$ ). The  $T=0$  value of  $\Theta$ ,  $\Theta_0=505$  K, as calculated from the elastic constants Eqs. (4) is shown also in Fig. 5, so, for the BR lattice, the  $\Theta(T)$  relation would rise sharply from 335 at 15 K to  $\Theta_0$  (505 K) at  $T=0$ . To emphasize this behavior, the normalized  $\Theta(T)$  for the nonquasicrystalline, nonmagnetic  $\xi'$  approximant of AlPdMn ( $-\square-$ )<sup>3</sup> also is shown. The  $\Theta(T)$  relation for  $i\text{-AlCuFe}$  (not shown) has a similar shape.<sup>5</sup> This abrupt departure from Debye behavior (constant  $\Theta$ ) on increasing temperature appears to be a basic characteristic of quasicrystalline and related materials, and implies that it is very difficult (impossible?) to obtain low temperature  $C_p$  parameters from fits of Eq. (2a) to a range of data for temperatures above 5 or 10 K.

$\Gamma(T)$  [Eq. (7), Fig. 6] plays the same normalized role for  $\alpha$  as  $\Theta(T)$  for  $C_p$ , and is a measure of the volume depen-

dence of the density of states and its variation with  $T$ . In spite of the almost factor of two differences in  $C_p$  and  $\alpha$  at low temperature in Figs. 4, the magnitudes of the  $\Gamma(T)$  relations for PRB and BR in Fig. 6 are very similar. This suggests that the  $\Gamma$  which is associated with the spin-glass state is similar in magnitude [6(1)] to the lattice  $\Gamma$ 's at low temperature. These  $\Gamma(T)$  relations are very similar to that for an AlCuFe quasicrystal in both temperature-dependence and relatively large magnitude, suggesting again a common quasicrystal characteristic.<sup>5</sup> These similar shapes can be associated with a large  $\Gamma$  for the high density of very low frequency modes which are responsible for the rapid decrease in  $\Theta(T)$  on warming.<sup>3,5</sup> A determination of the pressure-dependence of the elastic constants for AlPdMn<sup>36</sup> does not appear to support this hypothesis.<sup>3</sup>

Lattice contributions will be small at 1 K (Ref. 3), so the PRB/BR ratios of  $C_p$  (1.9) and  $\alpha$  (1.7) (Fig. 4) represent relative spin-glass contributions at 1 K. These ratios do not correlate directly with the factor of 4 ratio of the low temperature Curie parameters (C) in Table II. This difference may not be significant, since the  $C_p$  and  $\alpha$  data represent bulk sample averages, while the  $\chi$  data refer to a small fraction of the sample. Hippert *et al.*<sup>23</sup> show that small composition and significant  $\chi$  variations can occur along the growth axis of a Czochralski-grown sample. The present  $\chi$  data for the two halves (BRB, BRC) of the BR conductivity sample (Tables I and II, Figs. 2, and the end of Sec. III B) present another complication, since these data suggest that significant variations in the inhomogeneities which are associated with the Mn magnetism can exist over relatively large (mm) distances in a single grain sample. This is consistent with the report by Hartwig *et al.*,<sup>37</sup> that anomalous x-ray transmission data for a “highly perfect” single grain AlPdMn sample show the existence of a non-uniform distribution of bulk defects on a mm scale.

The close similarity of the compositions [Mn, 9.6(2)%] of the flux- and Bridgman-grown samples in this investigation (Table I) should minimize any effects due to the rather strong reported dependence of the susceptibility and spin-glass related properties on Mn composition.<sup>7,12</sup> The systematic study of Hippert *et al.*<sup>23</sup> includes the effects on  $\chi(T)$  of the structure, sample composition [Mn<sub>8,0(5)</sub>], method of preparation (Czochralski- and Bridgman-grown, rapidly cooled ribbons) and heat treatment (slow-cool, quench, intermediate anneal). After subtracting small  $\chi_0$  and ferromagnetic terms, the 5 to 150 K  $\chi(T)$  results for the various (19) samples could be made to coincide when a scaling factor,  $\mathbf{A}$ ,<sup>24</sup> was used, with  $\mathbf{A}=1$  for the  $\chi(T)$  of an arbitrarily chosen single grain material. The variation of  $\mathbf{A}$  for these samples ranged from 0.58 to 31.5. For comparison, single point (at  $1/T=0.15$  K<sup>-1</sup>) normalizations to this relation for the current (as grown) PRB and BR samples give  $\mathbf{A}=32$  and 4, respectively. In Ref. 23, the values of  $\mathbf{A}$  for as grown single crystal AlPdMn samples are 1.85 for a Bridgman sample (Mn<sub>8,0</sub>) and range from 7.45 to 31.5 for four as grown Czochralski samples [Mn<sub>8,5(2)</sub>]. While the differences between the present (quenched) PRB and (slow-cooled) BR  $\chi$ 's can be understood in terms of a smaller density of inhomogeneities (defects) for the BR sample, the differences between the Bridgman-grown

samples [1.85 (Ref. 23), 4 (present)] may represent a dependence on Mn composition; the differences from (and between) the as grown Czochralski single crystal samples appear to be large.

The above discussion has not included data for the two-phase annealed PRB (PRBAN) sample [Tables I and II and (•) in Figs. 3–6]. While PRBAN, when compared with the other samples, shows an enhanced magnetism above 100 K [Fig. 2(a)] and a relatively constant but smaller  $\chi$  below 10 K [Fig. 2(b)], the  $C_p$  and  $\alpha$  data are in reasonable agreement above approximately 20 K, and it is at lower temperatures that differences arise. These data have little inherent significance, since the physical properties of this sample cannot be characterized, although the relative insensitivity of the higher temperature data to sample structure and impurity also was found for icosahedral AlCuFe.<sup>5</sup> The data are presented here because, while  $\chi(T)$  in Fig. 2(a) could be described as “normal,” that in Fig. 2(b) is definitely unusual.

The origin of the two-phase state of the annealed PRB sample (PRBAN) also is of interest. It occurred in an attempt to transform PRB from its initial quenched-in HT icosahedral state to the equilibrium LT ( $F_{2M}$ ) state of the BR sample by slow cooling from 800°C to room temperature. When the data in Figs. 4 (•) were obtained, a subsequent metallographic examination of the sample revealed second phase inclusions (Table I). Boissieu *et al.*<sup>17</sup> have shown that for *i*-AlPdMn samples with Mn compositions similar to those in the present samples (9%), the structures and compositions of the two phases are slightly different. At 300 K equilibrium, the quenched-in HT phase is icosahedral (F1) with the composition Al<sub>68.8</sub>Pd<sub>22.0</sub>Mn<sub>9.2</sub>, while the LT phase is  $F_{2M}$ , with

the composition Al<sub>69.3</sub>Pd<sub>22.0</sub>Mn<sub>8.7</sub>, making it impossible for a single grain of one state to be annealed (or quenched) into a single grain of the other. To demonstrate this, a BR sample quenched from 800°C contained inclusions; when this sample then was annealed and slow-cooled to 300 K, the inclusions disappeared. This problem apparently does not exist for Mn compositions near 8%, where the LT phase is P-type.<sup>15,19</sup> Prejean *et al.*<sup>8</sup> report reversible behavior in the heat treatment (quenching vs slow annealing) of their [8.2(3)% Mn] samples, and no evidence of the unusual  $\chi(T)$  behavior which is shown in Fig. 2(b) for our two-phase sample PRBAN.

## ACKNOWLEDGMENTS

The authors wish to express their appreciation to Warren Strazheim for the SEM analyses of the sample compositions, and to Dr. Serguei Budko and Emilia Morosan for assistance in the susceptibility measurements. Notice: This manuscript has been authored by Iowa State University of Science and Technology under Contract No. W-7405-ENG-82 with the U.S. Department of Energy. The United States Government retains and the publisher, by accepting the article for publication, acknowledges that the United States Government retains a nonexclusive, paid-up, irrevocable, world-wide license to publish or reproduce the published form of this manuscript, or allow others to do so, for United States Government purposes. This manuscript has been authored by Iowa State University of Science and Technology under Contract No. W-7405-ENG-82 with the U. S. Department of Energy.

\*Electronic mail: swenson@ameslab.gov

†Present address: Los Alamos National Laboratory, Los Alamos, New Mexico 87545, USA.

<sup>1</sup>D. Schechtman, I. Blech, D. Gratia, and J. W. Cahn, *Phys. Rev. Lett.* **53**, 1951 (1984).

<sup>2</sup>A. P. Tsai, in *Physical properties of quasicrystals*, edited by Z. M. Stadnik (Springer, New York, 1999).

<sup>3</sup>C. A. Swenson, I. R. Fisher, N. E. Anderson, Jr., P. C. Canfield, and A. Migliori, *Phys. Rev. B* **65**, 184206 (2002).

<sup>4</sup>I. R. Fisher, M. J. Kramer, T. A. Wiener, Z. Islam, A. R. Ross, T. A. Lograsso, A. Kracher, A. Goldman, and P. C. Canfield, *Philos. Mag. B* **79**, 1673 (1999).

<sup>5</sup>C. A. Swenson, T. A. Lograsso, A. R. Ross, and N. E. Anderson, Jr., *Phys. Rev. B* **66**, 184206 (2002).

<sup>6</sup>M. A. Chernikov, A. Bernasconi, C. Beeli, A. Schilling, and H. R. Ott, *Phys. Rev. B* **48**, 3058 (1993).

<sup>7</sup>J. C. Lasjaunias, A. Sulpice, N. Keller, J. J. Préjean, and M. de Boissieu, *Phys. Rev. B* **52**, 886 (1995).

<sup>8</sup>J. J. Préjean, C. Berger, A. Sulpice, and Y. Calvayrac, *Phys. Rev. B* **65**, 140203(R) (2002).

<sup>9</sup>M. de Boissieu, M. Durand-Charre, P. Bastie, A. Carabelli, M. Boudard, M. Bessiere, S. Lefebvre, C. Janot, and M. Audier, *Philos. Mag. Lett.* **65**, 147 (1992).

<sup>10</sup>Y. Yokoyama, T. Miura, A.-P. Tsai, Akihisa, and T. Masumoto,

*Mater. Trans., JIM* **33**, 97 (1992).

<sup>11</sup>M. Boudard, E. Bourgeat-Lami, M. de Boissieu, C. Janot, H. Klein, M. Audier, M. Durand-Charre, and B. Hennion, *Philos. Mag. Lett.* **71**, 11 (1995).

<sup>12</sup>P. Lanco, T. Klein, C. Berger, F. Cyrot-Lackmann, G. Fourcaudot, and A. Sulpice, *Europhys. Lett.* **18**, 227 (1992).

<sup>13</sup>T. Ishimasa and M. Mori, *Philos. Mag. B* **66**, 513 (1992).

<sup>14</sup>M. Audier, M. Durand-Charre, and M. de Boissieu, *Philos. Mag. B* **68**, 607 (1993).

<sup>15</sup>T. Ishimasa, *Philos. Mag. Lett.* **71**, 65 (1995).

<sup>16</sup>D. Häussler, C. Beeli, and H.-U. Nissen, *Philos. Mag. Lett.* **75**, 117 (1997).

<sup>17</sup>M. de Boissieu, M. M. Boudard, T. Ishimasa, E. Elkaim, J. P. Lauriat, A. Letoublon, M. Audier, M. Duneau, and A. Davroski, *Philos. Mag. A* **78**, 305 (1998).

<sup>18</sup>M. Audier, M. Duneau, M. de Boissieu, M. Boudard, and A. Letoublon, *Philos. Mag. A* **79**, 255 (1999).

<sup>19</sup>T. Ishimasa, in *Proceedings of the 5th International Conference on Quasicrystals, Avignon, France*, edited by C. Janot and R. Mosseri (World Scientific, Singapore, 1995), p. 648.

<sup>20</sup>A. Kobayashi, S. Matsuo, T. Ishimasa, and H. Nakano, *J. Phys.: Condens. Matter* **9**, 3205 (1997).

<sup>21</sup>S. Matsuo, T. Ishimasa, and H. Nakano, *Solid State Commun.* **102**, 575 (1997).

- <sup>22</sup>A. A. Rempel, S. Z. Nazarova, and A. I. Gusev, *JETP Lett.* **72**, 144 (2000).
- <sup>23</sup>F. Hippert, M. Audier, J. J. Prjean, A. Sulpice, E. Lhotel, V. Simonet, and Y. Calvayrac, *Phys. Rev. B* **68**, 134402 (2003).
- <sup>24</sup>The parameter (**A**) is used in this paper for the scaling factor, since that used in Ref. 23 ( $\alpha$ ) refers here to the linear thermal expansivity.
- <sup>25</sup>A. R. Ross, T. A. Wiener, I. R. Risher, P. C. Canfield, and T. A. Lograsso, *Mater. Sci. Eng., A* **294–296**, 53 (2000).
- <sup>26</sup>A. R. Ross, I. R. Fisher, T. A. Lograsso, and P. C. Canfield, in *Quasicrystals*, edited by R. Belin-Ferré, P. A. Thiel, A-P Tsai, and K. Urban, Materials Research Society Symposia Proceedings, 643, p. K1.5.1 (2001).
- <sup>27</sup>C. A. Swenson, *Rev. Sci. Instrum.* **70**, 2728 (1999).
- <sup>28</sup>C. A. Swenson, in *Thermal Expansion of Solids*, edited by C. Y. Ho and R. E. Taylor, Chap. 8 in Vol. **I-4** of the CINDAS Data Series on Material Properties (ASM, 1998).
- <sup>29</sup>W. A. Phillips, *Rep. Prog. Phys.* **50**, 1657 (1987).
- <sup>30</sup>E. S. R. Gopal, *Specific Heats at Low Temperatures* (Plenum, New York, 1966).
- <sup>31</sup>The ratios  $B_S/B_T$  and  $C_P/C_V$  are given by  $C_P/C_V=B_S/B_T=[1+\beta^2B_SV/C_P T]=[1+\beta\Gamma T]$ , where  $\beta=3\alpha$  and  $\Gamma$  is the Grüneisen parameter which is described in Sec. III C. This ratio is 1.004 and negligible at the present highest temperature, 108 K (see Ref. 3), so no distinction will be made between  $C_P$  and  $C_V$  when discussing the present data.
- <sup>32</sup>T. H. K. Barron, in *Thermal Expansion of Solids*, edited by C. Y. Ho and R. E. Taylor, Chapter 1 in Vol. **I-4** of the CINDAS Data Series on Material Properties (ASM, 1998).
- <sup>33</sup>T. H. K. Barron, J. G. Collins, and G. K. White, *Adv. Phys.* **29**, 609 (1980).
- <sup>34</sup>M. A. Chernikov, E. Felder, A. D. Bianchi, C. Wälti, M. Kenzelmann, H. R. Ott, K. Edagawa, M. de Boissieu, C. Janot, M. Feuerbacher, N. Tamura, and K. Urban, in *Proceedings of the 6th International Conference on Quasicrystals, Avignon, France*, edited by S. Takeuchi and T. Fujiwara (World Scientific, Singapore, 1998), p. 451.
- <sup>35</sup>J. C. Lasjaunias, Private Communication (2000).
- <sup>36</sup>Y. Amazit, M. Fischer, B. Perrin, A. Zarembowitch, and M. de Boissieu, *Europhys. Lett.* **25**, 441 (1994).
- <sup>37</sup>J. Hartwig, S. Agliozzo, J. Baruchel, R. Colella, M. de Boissieu, J. Gastaldi, H. Klein, L. Mancini, and J. Wang, *J. Phys. D* **34**, A103 (2001).